Clinical Neuroimaging Using 7 T MRI: Challenges and Prospects

Maria Isabel Vargas, Pascal Martelli, Lijing Xin, Ozlem Ipek, Frederic Grouiller, Francesca Pittau, Robert Trampel, Rolf Gruetter, Serge Vulliemoz, Francois Lazeyras

From the Division of Neuroradiology of Geneva University Hospitals and Geneva University, Geneva, Switzerland (MIV); Animal Imaging and Technology Core (AIT), Center for Biomedical Imaging (CIBM), Ecole Polytechnique Fédérale de Lausanne, Lausanne, Switzerland (PM, LX, OI, RG); CIBM, Department of Radiology and Medical Informatics, Geneva Hospitals and University of Geneva, Geneva, Switzerland (FG, FL); Division of Neurology, Epileptology Unit, Geneva University Hospitals, Geneva, Switzerland (FP, SV); Max Planck Institute for Human Cognitive and Brain Sciences, Leipzig, Germany (RT); and Division of Radiology of Geneva University Hospitals and CIBM, Geneva, Switzerland (FL).

ABSTRACT

The aim of this article is to illustrate the principal challenges, from the medical and technical point of view, associated with the use of ultrahigh field (UHF) scanners in the clinical setting and to present available solutions to circumvent these limitations.

We would like to show the differences between UHF scanners and those used routinely in clinical practice, the principal advantages, and disadvantages, the different UHFs that are ready be applied to routine clinical practice such as susceptibility-weighted imaging, fluid-attenuated inversion recovery, 3-dimensional time of flight, magnetization-prepared rapid acquisition gradient echo, magnetization-prepared 2 rapid acquisition gradient echo, and diffusion-weighted imaging, the technical principles of these sequences, and the particularities of advanced techniques such as diffusion tensor imaging, spectroscopy, and functional imaging at 7TMR.

Finally, the main clinical applications in the field of the neuroradiology are discussed and the side effects are reported.

Keywords: 7TMR, UHF, epilepsy, neuroradiological imaging, brain.

Acceptance: Received August 8, 2017. Accepted for publication October 2, 2017.

Correspondence: Address correspondence to Maria Isabel Vargas, MD, Division of Neuroradiology, DISIM, Geneva University Hospitals, Rue Gabrielle-Perret-Gentil 4, 1211 Genève 14, Switzerland. E-mail: maria.i.vargas@hcuge.ch.

Acknowledgment and Disclosure: This work was supported by the Department of Radiology of Geneva University Hospitals (HUG) Fund startup 2013-10 "Détection des lésions épileptogènes du manteau cortical à 7T" and by the Swiss National Science Foundation (SNSF) grants 141165, 140332 (SPUM Epilepsy), as well as the Centre d'Imagerie Bio-Médicale (CIBM), the Swiss Federal Institute of Technology Lausanne (EPFL), and Lausanne and Geneva Hospital and University.

The authors report no conflicts of interest.

J Neuroimaging 2018;28:5-13.
DOI: 10.1111/jon.12481

Introduction

In the last decade, advances in medical imaging have revolutionized the diagnosis and treatment of diseases of the central and peripheral nervous systems. The introduction of high-strength magnetic field (3 tesla) in magnetic resonance imaging (MRI) has allowed the visualization of small structures in exceptional detail.

7 T MR is the next natural step in the clinical setting; however, it is not currently widely used yet. Only sixty-one 7 T MRI scanners are in function around the world.[1] Few centers have begun to use this technique that has been limited to selected patients with certain pathologies such as multiple sclerosis (MS),[2] epilepsy,[3] tumors,[4,5] to evaluate the effects of radiotherapy on normal appearing brain in patient with gliomas,[4] neurodegenerative diseases, and vascular pathologies (Fig 1).[4,6]

A higher static magnetic field strength offers various advantages for in vivo applications such as increased signal-to-noise ratio (SNR),[7,8] which can be translated to higher spatial resolution for structural and functional MR,[3,9] increased chemical shift dispersion,[10] and improved sensitivity in T2*-weighted blood oxygenation-level-dependent (BOLD) imaging.[11] Magnetic susceptibility-weighted techniques also benefit from ultrahigh field (UHF) strength imaging as it allows visualization of small anatomical structures based on susceptibility differences between blood, iron, and myelin.

On the other hand, increased main magnetic field inhomogeneity, B1 inhomogeneity, and artifacts represent new challenges.

In this review, we aim to illustrate the sequences that are ready at UHF to be applied to routine clinical practice, new artifacts, some of the challenges inherent to UHF, and a more accurate assessment of metabolites by MR spectroscopy (MRS).

Clinical Applications

The anatomical regions most likely to benefit from UHF are the central nervous and musculoskeletal systems. This is due to the fact that structures in these systems are relatively unaffected by cardiac and breathing motion, which allows us to use sequences with higher spatial resolution that need a longer acquisition time.

For the brain, the principal clinical applications are related to the high resolution with which anatomical structures can be depicted,[1,2] improved contrast, reduced quantity of contrast medium used, and new sequences that are likely to be developed in the future[5] (Fig 2).

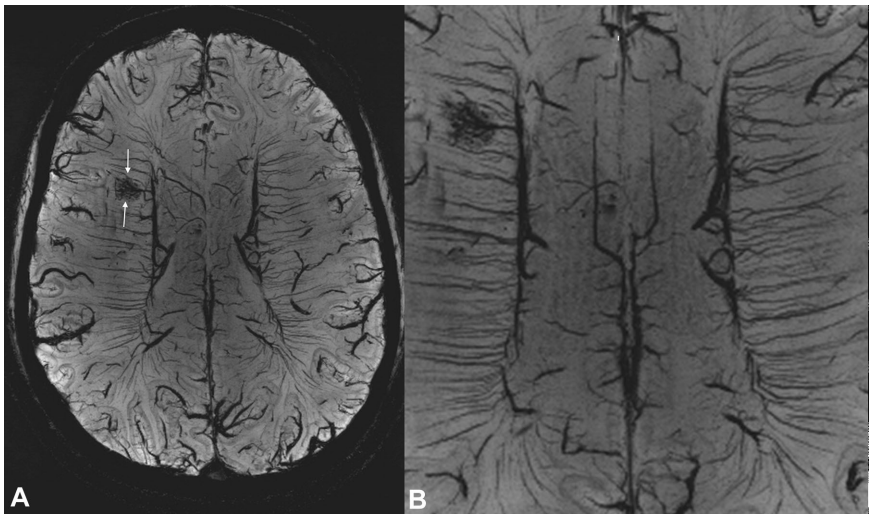

Fig 1. Axial susceptibility-weighted imaging (TR 28 milliseconds, TE 20 milliseconds, flip angle 10, voxel size .4 × .4 × 1 mm, acquisition time 5 minutes) nicely illustrates the small, irregular, and enlarged vessels in this patient with a capillary telangiectasia of the frontal lobe (A, arrows). A zoomed image (B) shows a remarkable depiction of the normal transmedullary veins on both sides of the cerebral hemispheres.

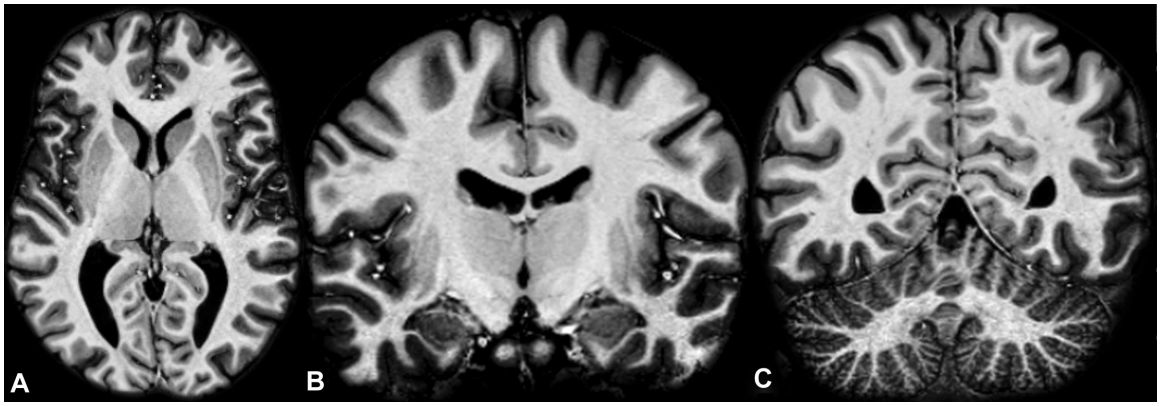

Fig 2. Axial and coronal high-resolution magnetization-prepared two rapid acquisition gradient echo (TR 6000 milliseconds, TE 3.1 milliseconds, IT 1,800 milliseconds, IT2 2,700 milliseconds, .6 mm isotropic resolution, acquisition time 10 minutes) of a 28-year-old volunteer. Note the excellent delineation of the different components of the basal ganglia in (A) and (B). Full coverage of the brain in (C). Note also the high contrast between gray and white matter in (A) to (C).

The pathologies that could benefit from 7 T MRI include MS,[2,12–15] tumors,[5] epilepsy[3] (Figs 3a, 3b, 4, 5), neurodegenerative, and vascular diseases and those that require functional imaging.[4]

The high anatomical resolution can be used to obtain higher precision in the planning of electrode positioning in the treatment of Parkinson disease and epilepsy or in the ablation of tumors.[1]

Seven tesla imaging will provide a better understanding of the pathophysiology of different types of tumors, in part, due to improved identification and characterization of low-grade and high-grade areas of infiltration, the interface between edema and tumor, and changes in tumor permeability,[5] particularly with the help of susceptibility imaging, which should directly impact on tumor classification and planning of treatment (better identification of biopsy targets).[16]

This will furthermore help understand tumor response and side effects of treatment. In epilepsy, the detection and characterization of subtle lesions can be of critical importance for patient management, especially for patients who suffer from medically refractory epilepsy and are candidates for surgery. Indeed, the detection of a structural lesion largely increases the odds of favorable postoperative seizure control, by guiding resection or the placement of intracranial electrodes for invasive monitoring.

Seven tesla imaging can guide treatment as it is currently possible to visualize the hippocampi and their microstructure; different articles illustrate various anatomical structures such as the subiculum and Cornu Ammonis (CA), CA1, CA2, CA3, and CA4 (Figs 3a and 3b).[16] Focal cortical dysplasia, the most common cause of medically refractory epilepsy in children and also frequent in adults, can also be very difficult to detect even with 3 T imaging. Postoperative outcome is increased by total resection of the lesion. A better detection and delineation of these lesions at 7 T would therefore be very useful. Small posttraumatic lesions could also be better detected at 7 T.

UHF increases the detection rate and improves characterization of cortical, thalamic and leptomeningeal lesions, and

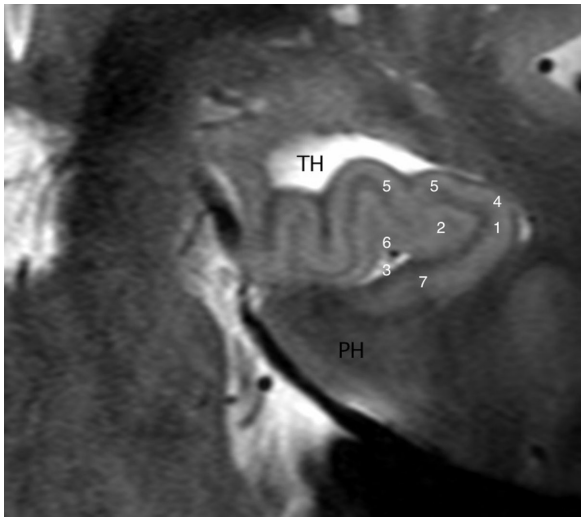

Fig 3a. Coronal high-resolution T2 showing different regions of the hippocampus. Note the exceptional differentiation between white and gray matter. 1. Hippocampal head. 2. Gyrus dentatus. 3. Uncal sulcus. 4. Cornu Ammonis. (CA)1, 5. CA2 3, 6. CA4. TH = temporal horn; PH = parahippocampal gyrus.

their contribution to cognitive decline in MS.[12,13] Magnetic susceptibility sequences allow visualization of small caliber blood vessels at the center of white matter lesions and they improve visualization of lesions of the cervical and upper dorsal spine cord due to high spatial resolution.[14,15,17]

Furthermore, magnetic susceptibility imaging can play a key role in identifying patients at risk of bleeding, for example, those with arteriovenous malformations in which treatment is controversial and also to determine the risk of rupture of aneurysms by studying the vascular wall.[18]

Adverse Effects

Side effects of UHF-MRI include vertigo, the main complaint at UHF according to Theysohn et al,[19] followed by nausea, light flashes, metallic taste in the mouth, too much noise during image acquisition, and discomfort. De Vocht et al reported a decreased performance on cognitive tests with no effects perceived on the working memory.[20] Furthermore, no significant changes in vital signs have been demonstrated.[21]

Acquisition time is still a real limitation; gradient recalled echo (GRE)-based sequences such as magnetization-prepared rapid acquisition gradient echo (MPRAGE), magnetization-prepared 2 rapid acquisition gradient echo (MP2RAGE), or SPoiled Gradient Recalling imaging (SPGR) allow a full coverage of the brain in a reasonable time for clinical applications. Applications of spin echo (SE)-based sequences, however, have several limitations due to specific absorption rate (SAR) constrains that limit the number of slices available per unit of time. In order to achieve a reasonable acquisition time for clinical examination, small spatial coverage in the slice direction is obtained. However, remarkable image quality can be obtained in brain regions defined beforehand by other means such as electroencephalogram (EEG), clinical information, or other MRI sequences.

The higher spatial resolutions that are possible at UHF increase scan time as a result, which can result in patient discomfort. Additionally, it may be necessary to extend measurement time due to the higher SAR at field strengths of 7 T, which is a problem particularly for sequences comprising high radio frequency (RF) power pulses, such as T2-weighted imaging (WI) spin echo or fluid-attenuated inversion recovery (FLAIR) using turbo spin echo/fast spin echo (TSE/FSE) readout. Multiarray coils in combination with parallel imaging can accelerate the acquisition resulting in reasonable scan times for clinical studies. Furthermore, new methods were developed lately to overcome

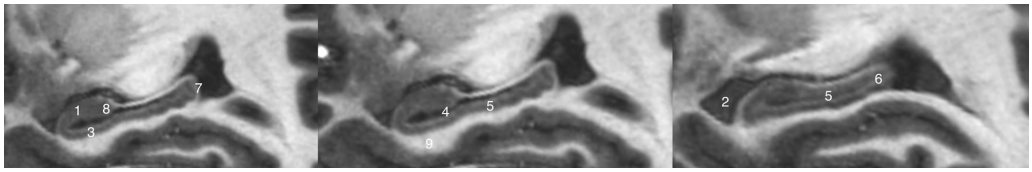

Fig 3b. Sagittal magnetization-prepared two rapid acquisition gradient echo image shows different regions of the hippocampus. Note the exceptional differentiation between white and gray matter. 1. Hippocampal head. 2. Temporal horn. 3. Subiculum. 4. Uncal sulcus. 5. Hippocampal body. 6. Hippocampal tail. 7. Alveus. 8. Gyrus dentatus.

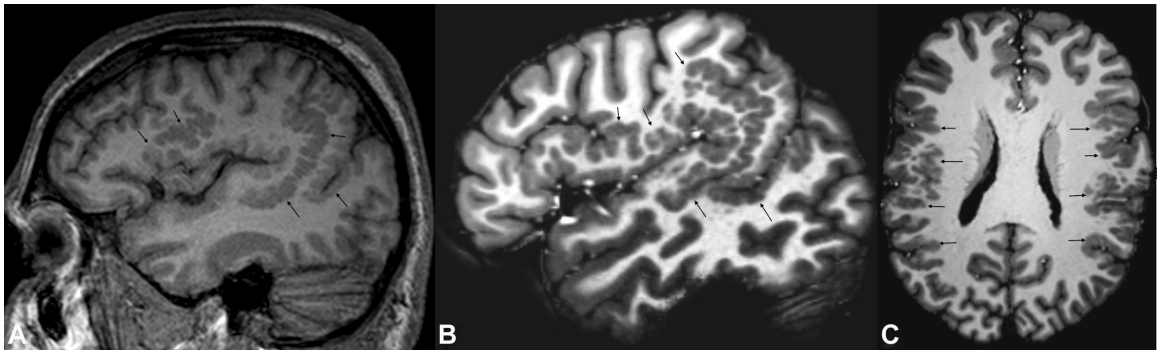

Fig 4. A 20-year-old patient known for focal epilepsy due to bilateral fronto-parietal and temporal polymicrogyria. (A) shows polymicrogyria on sagittal 3-dimensional T1 at 3 T. In (B) and (C), the magnetization-prepared 2 rapid acquisition gradient echo sequence at 7 T clearly shows a much better delineation of polymicrogyria due to improved contrast between gray and white matter.

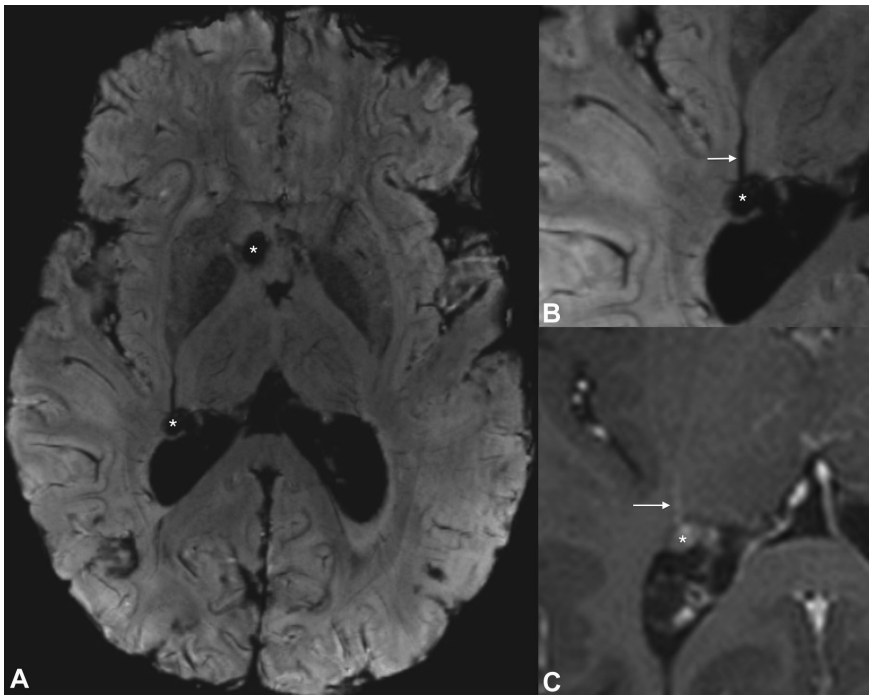

Fig 5. A 24-year-old patient with tuberous sclerosis. Subependymal nodules are well visualized as hypointense round abnormalities adjacent to the right lateral ventricle (*) on axial susceptibility-weighted imaging. Zoomed image (B) shows a vein in contact with the nodule (arrows) almost invisible on axial spin echo T1 at 3 T with contrast.

SAR limitation for TSE implementation. For instance, reduction of SAR level on 2-dimensional TSE can be achieved using gradient and spin echo (GRASE) or RF subpulses.[22,23] Three-dimensional T2-weighted sequences are also promising;[24] however, these different methods are not yet sufficiently developed to be used in clinical routine.

Anatomical models have been utilized to calculate the induced current density and SAR in adults, children, pregnant woman, and fetuses. The effects change with age, the tissues most affected in adults and children by the high SAR being cerebrospinal fluid (CSF), the skin, and gray matter.[25]

The use of UHF is difficult in children as side effects are particularly difficult to tolerate in this age group. There is only one report in the literature dedicated to 7 T MRI in children and no studies have proven the complete safety of this type of exam if performed repeatedly.

Sequences

Images acquired on 7 T scanners have incomparable spatial resolution and definition, particularly those produced by susceptibility-weighted imaging (SWI). Although the fundamental architecture of sequences used at 7 T is the same as on 3 T scanners (MPRAGE, MP2RAGE, SPGR, SE T2, FLAIR, SWI, diffusion tensor imaging [DTI], 3-dimensional time of flight [TOF], and spectroscopy), significant improvements and parameter adjustments are still necessary to bring 7 T MRI into routine clinical practice. The most common sequences currently used in clinical practice and issues relating to optimization of these sequences are dealt with in the next section.

T1 Weighted

The most common technique for acquiring T1-weighted images at 7 T is the MPRAGE sequence. Despite being widely used at 3 T, at higher field strength, MPRAGE images are inhomogeneous due to B1 variations, which may impair clinical interpretation. One approach is to use two inversion times (ITs) (MP2RAGE), which has the advantage of producing bias-free images with high contrast between gray and white matter in addition to a robust T1 mapping (Figs 2 and 3b, and 4).[26]

Fluid-Attenuated Inversion Recovery

FLAIR is a pulse sequence that nulls tissue or fluid signal by applying an inversion pulse before signal acquisition. By carefully choosing the IT, the signal from any particular tissue can be canceled; in clinical MR, it is mostly used to suppress CSF.

FLAIR is used to detect/diagnose a wide range of central nervous system diseases and offers an increased sensitivity when compared to T1 and T2 images in the evaluation of stroke, MS, infection, and toxic and metabolic diseases. T2-weighted FLAIR imaging is currently one of the cornerstones of MR neuroimaging protocols in the clinical setting at 1.5 and 3 T.[27]

The contrast of gray/white matter does not necessarily increase with the field strength.[28] This is due to the lengthening of T1-values of gray and white matter at UHF, while the T1 of CSF is relatively field-independent, leading to compromised T2-contrast and reduced magnetization recovery at the moment of excitation. To overcome this problem, a UHF version of FLAIR was developed comprising a magnetization preparation module that effectively leads to an inversion recovery of the CSF but only to a saturation of gray and white matter.[29]

Diffusion-Weighted Imaging and Diffusion Tensor Imaging

Diffusion-weighted imaging (DWI) allows the noninvasive visualization of anatomical connections between different parts of the brain by mapping the diffusion process of water molecules

in biological tissues. The first diffusion MRI images were produced in the mid-1980s and were used soon after in the clinical setting.

Diffusion and DTI are widely used in the field of neuroradiology for the study and to guide treatment of diseases such as stroke, infections, etc. DTI is particularly successful because it reveals the brain connectivity and abnormalities/lesions in white matter fiber structure. Diffusion images, tractography, and more specifically fractional anisotropy profit greatly of a higher magnetic field where the resolution is paramount. However, increased distortion by field inhomogeneity at UHF remains a challenge that needs to be overcome in order to fully benefit from the UHF potential.[30] Some new approaches are being explored such as readout-segmented echo planar imaging (EPI) together with motion correction showing promising results.[31,32]

Susceptibility-Weighted Imaging

SWI is an MRI technique that exploits the local magnetic field differences between tissues.[33,34] SWI is based on a fully flow-compensated 3D high-spatial resolution GRE that combines magnitude and unwrapped phase images to produce an enhanced contrast magnitude image. By increasing the field strength, it enables the use of shorter echo times (TE) while maintaining the same phase difference, and along with a higher SNR, it improves resolution and speed.[1,35]

Unfortunately, the field patterns seen in phase images are nonlocal due to small local susceptibility distributions. Thus, the phase images do not necessarily reflect anatomical structures locally and the contrast depends on the orientation of the object in relation to the main magnetic field.[36] Care must therefore be taken when relating the phase contrast (PC) to brain anatomy, especially in regions of complicated anatomy such as the basal ganglia. Quantitative susceptibility mapping (QSM) overcomes this problem and might therefore replace SWI at UHF even in clinical settings, despite the technical and mathematical challenges.[37]

Currently, the most common indications are for the detection of microhemorrhages, calcifications, iron accumulation, and the visualization of vascular structures, particularly veins[38] (Figs 1 and 5).

3D TOF Angiography

Three-dimensional TOF is obtained routinely with clinical MRI at 1.5 and 3 T for detection of thrombus, plaques of atheroma, vasculitis, and aneurysms at high resolution with a coverage of 10 cm and a resolution of .3 × .3 × .5 mm^3.

At UHF, technical parameters are: FOV 200 × 190 × 50 mm^3 in transverse orientation and acquired voxel size .25 × .3 × .4 mm.

Recent studies have illustrated the benefits of 7 T in the analysis of intracranial vessels with and without contrast,[39] allowing the visualization of the whole circle of Willis and intracranial perforating arteries. However, venous contamination has been reported with both techniques.[40,41] Brain coverage is reduced by constraints of SAR and can result in long acquisition times that are difficult to apply in clinical routine.[6]

Finally, the new sequence MPRAGE-MRA seems to decrease the acquisition time with higher resolution.[42]

1H Magnetic Resonance Spectroscopy

1H MRS allows the noninvasive measurement of neurochemical information in the human brain. With the increase of magnetic field strength ≥7 T, high spectral resolution (eg, improved separation of glutamate and glutamine) and SNR would largely improve the quantification for metabolites, reduce acquisition time, and increase spatial resolution[43] (Figs 6 and 7). However, there are a number of technical challenges such as increased B0, B1 field inhomogeneities (discussed below in the "challenges/solutions" section), chemical shift displacement (CSD) due to volume selection, reduced T2 relaxation times, and increased T1 relaxation times.

Individual metabolites actually experience different excitation volumes due to their difference in chemical shift.

Despite the potential of UHF in spectroscopy, few clinical applications have been reported and include the localization of the epileptogenic zone in medically refractory epilepsy and tumor lesions. The fact that higher field strength yields better SNR and improved spectral resolution allows better metabolite depiction. In epilepsy, the added value of UHF is the possibility to measure glutamate and glutamine separately and also more accurate assessment of gamma-amino butyric acid (GABA), which can bring new insights into the detection of epileptic lesions. For tumor assessment, improved spatial resolution may improve the differentiation of edema from low-grade infiltration and also characterization of lesions.[44]

Functional MRI

Noninvasive mapping of functional brain functions can be achieved by functional MRI (fMRI) that allows the detection of hemodynamic changes associated with cerebral activity. The most standard method is the BOLD effect depending on the paramagnetic properties of deoxyhemoglobin that induce local modifications of the magnetic susceptibility.[45]

BOLD signal sensitivity increases linearly with field strength opening the possibility to critically enhance spatial resolution or to decrease the number of repetitions to obtain significant BOLD changes at UHF.[46,47] Furthermore, the intravascular contribution from large vessels to BOLD signal decreases with magnetic field strength offering a better spatial specificity at higher field by reducing the signal from draining veins.[48]

These significant benefits in BOLD signal sensitivity and specificity at UHF make clinical fMRI at 7 T the technique of choice for non-invasive mapping of language or motor cortex to be preserved during surgery.[49] In patients with medically refractory epilepsy, presurgical mapping can be enriched by simultaneous EEG-fMRI that can be performed safely at 7 T in order to noninvasively localize hemodynamic correlates of interictal epileptic activity during presurgical investigations.[3]

Coils

The excellence of UHF MR imaging quality depends ultimately on RF coil performance. The increase in the static magnetic fields brings new physical challenges: decreased RF penetration in a subject,[7,50] higher RF power requirements,[51] and increase in susceptibility artifacts.[52] Even more importantly, the RF wavelength in the body becomes comparable or smaller in size than the anatomical dimensions, which can lead to interference patterns. While destructive interference leads to darkening of the image, constructive interference may lead to local brightening

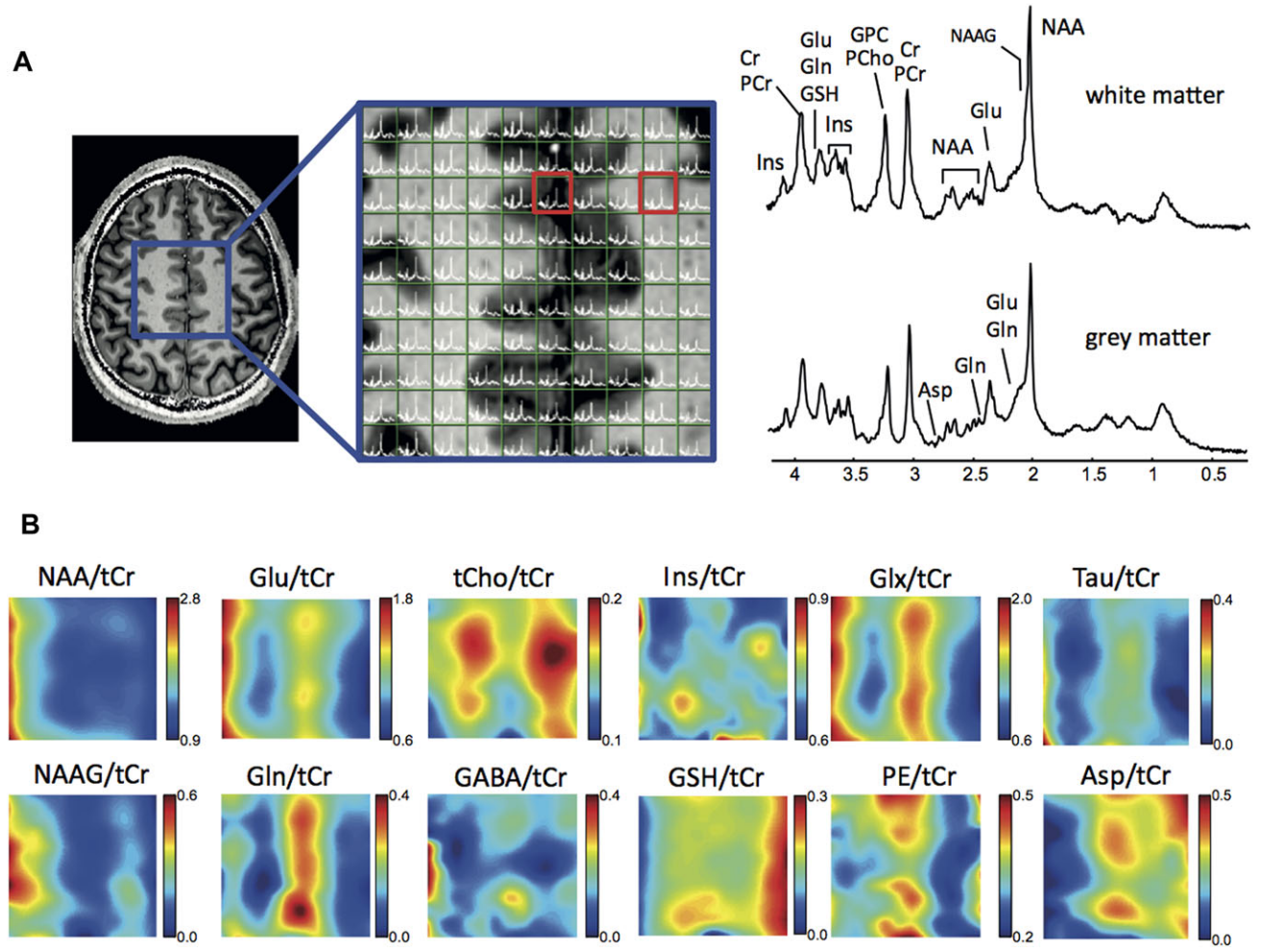

Fig 6. (A) Left: transverse MR image of a brain with the selected volume of interest (VOI) for spectroscopic imaging indicated by the blue square; Middle: enlarged spectra maps in VOI; Right: representative spectra from a voxel containing gray matter and white matter, respectively (red boxes in the middle image). (B) Maps of relative concentrations to total creatine (tCr) (echo time/repetition time = 16/4,000 milliseconds, field of view = 190 × 190 mm^2, VOI = 70 × 70 mm^2, slice thickness = 10 mm, matrix = 20 × 20, number of excitations = 1, interpolate = 32 × 32, elliptical *k*-space sampling, nominal resolution = 9.5 × 9.5 × 10 mm^3). NAA = N-acetylaspartate; Cr = creatine; PCr = phosphocreatine; Lac = lactate; GABA = gamma-amino butyric acid; GSH = glutathione; GPC = glycerophosphocholine; TAU = taurine; INS = myo-inositol; PE = phosphoethanolamine; ASP = aspartate; Glu = glutamate; Gin = glutamina; Glx = Glutamate-Glutamine; NAAG = N-Acetylaspartylglutamate. Numbers on the graph express the resonant frequencies in parts per million (ppm).

of the image. Therefore, at UHF MR imaging, a strong contribution of the induced conductive and dielectric currents to RF-induced signal variations across the subject is highly visible.

Compared to more conventional 3 T MR systems, achievable B1 (transient B1) fields are also limited by less powerful RF power amplifiers (2 Å-15 kW at 3 T, compared to 2 Å-4 kW at 7 T) and inherently higher cable losses. This results in a situation where RF power demanding sequences such as spin echo sequences face challenges with respect to sufficiently available B1 and imaging speed due to increased RF heating concerns in the body.

UHF enables improved sensitivity and encoding capabilities of fMRI. The introduction of multiple receiver arrays showed the sensitivity benefit of receiving the MR signal with multiple smaller coils.[53] Reduced acquisition times are not only favorable in reducing the impact of subject motion, but also allow functional measurements in the same subject and in the same measurement session, which is ideal for studying the relation between anatomy and function.

Acquiring whole-brain T2-weighted images at 7 T is challenging due to both visible inhomogeneous transmit patterns in the image and power deposition limitations. However, combining parallel transmit methods with SAR and scan time reducing approaches may overcome this problem.[54]

Another challenge at UHF head imaging is tissue heating, which is a result of time-varying magnetic-field-induced electric fields in a subject according to Maxwell's equations. The electric field induces currents in a subject, which leads to tissue heating in the case of a conductive tissue. SAR limit relevant to the UHF imaging RF coils is 10 W/kg for averaged over 10 g of tissue according to IEC 60601-2-33 (IEC, 2010) guidelines.

A crucial goal in increasing the main field strength is to achieve molecular-level high resolution to understand the brain further. Currently, the sensitivity of available RF coils is limited for microscopic imaging without administration of a contrast agent to a subject. Molecular-level imaging is possible only with the application of a specialized molecular sensor.[55]

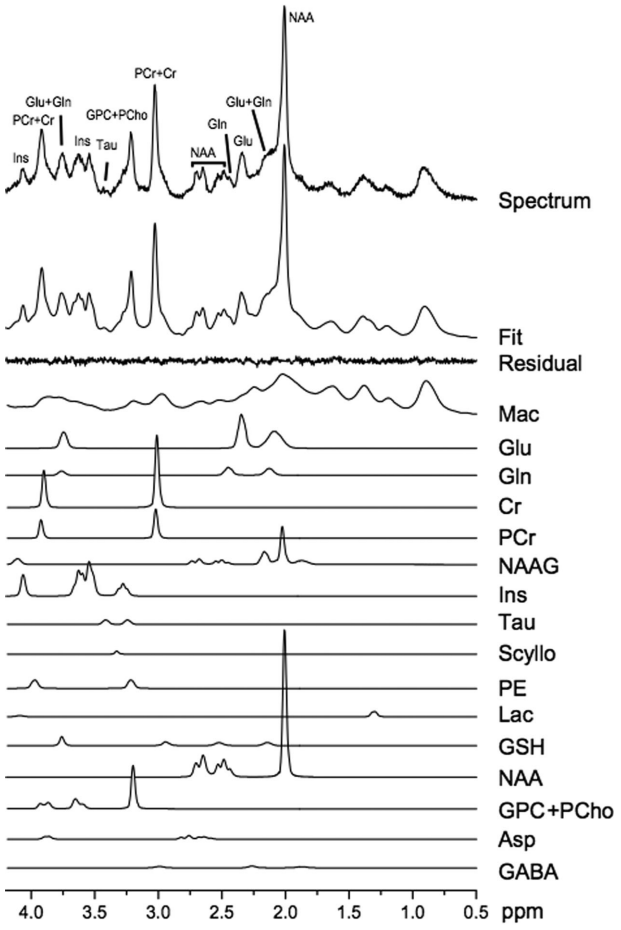

Fig 7. In vivo ^{1}H MR spectrum acquired using semiadiabatic SPECIAL localization sequence (TE/TR = 12/7,500 milliseconds, 32 averages) from a volume of interest (20 × 15 × 20 mm^3) in the occipital lobe of a healthy volunteer and its LC model fit, fit residual, and the individual metabolite fits. Lac = lactate; GABA = gamma-amino butyric acid; NAA = N-acetylaspartate; Glu = glutamate; Gln = glutamine; Asp = aspartate; Cr = creatine; PCr = phosphocreatine; GPC = glycerophosphocholine; Tau = taurine; Ins = myo-inositol; GSH = glutathione; PCho = phosphocholine; NAAG = N-Acetylaspartylglutamate; PE = phosphoethanolamine; Mac = macromolecule baseline. Numbers on the graph express the resonant frequencies in parts per million (ppm).

Challenges/Solutions

Current use of UHF MR imaging is limited by technical issues including inhomogeneities of both the main magnetic field (B0) and the applied RF field (B1), the SAR, and changes in relaxation times compared to lower field strengths. These limitations cause image artifacts, limit temporal and spatial resolution and/or coverage, and restrict the use of MR spectroscopy. Solutions for these technical issues include parallel transmit techniques and customized RF pulse sequences to produce a uniform transmission while minimizing deposited RF energy (SAR) or parallel imaging to reduce the scanning time.

Inhomogeneities

All sequences should benefit from the increased SNR. However, when moving toward UHF, inhomogeneities appear in the B0 and B1 fields.[56]

Both image geometry and intensity of signal are distorted with B0 inhomogeneities, which increase linearly with the field strength. For MR spectroscopy, inhomogeneous B0 field may result in shifting and broadening of the spectral lines of metabolites, leading to insufficient water and lipid saturation and degradation in SNR and spectral separation.

Currently, automatic corrections are fully integrated in the prescan procedure and are available in most commercially available MR systems. Automatic shimming methods include AUTOSHIM,[57] FASTMAP,[58] and are the most used clinically.

Another main challenge at 7 T is B1 inhomogeneities leading to artificial signal differences across the brain for all common MR contrasts and it is most severe for T2-weighted sequences, such as SE and TSE. The most significant change is between the overexposed area in the center of the brain and the periphery. For MRS, B1 inhomogeneities can lead to insufficient peak power for the surface region of the brain, imperfections of the excitation/refocusing slice profile, and the excitation of unwanted signal originating outside the volume to interest.

These variations in B1 occur because RF wavelength approaches the size of the body part being imaged (head, chest, and abdomen), therefore causing interferences. This leads to a loss of signal and unexpected changes in contrast in anatomical and spectroscopic images, which may ultimately result in the misinterpretation of results. The use of parallel transmitters,[59] barium titanium-based dielectric pads,[60,61] and specific RF pulse design have been proposed to mitigate the B1 inhomogeneity occurring at high field strength.[62]

Specific Absorption Rate

Tissue heating caused by the absorption of radio waves is another important challenge. RF power deposition, measured as the SAR, increases exponentially with the magnetic field strength. Although, in practice, some other aspects may help counterbalance this problem, SAR restrictions are more limiting compared to lower field strengths, requiring a reduction in the number, duration, and amplitude of applied RF pulses in a given time period.[4]

In pulse sequences that use many high flip angle RF pulses, such as fast/turbo spin-echo and FLAIR, the SAR limit is quickly reached.[63] The first option to avoid an increasing SAR is by distributing the flip angles over a larger time period (longer TR), but in a clinical setting, time is a costly resource. Parallel imaging combined with a lower flip angle schedule can be used to reduce the acquisition time.[64]

Adapted RF pulse design (modification in frequency and in amplitude/phase of the B1+ field) can minimize and sometimes settle the hardware/physical limitations so that gain in signal intensity of UHF is available. The implementation of adiabatic pulses, which are less sensitive to B1 field variations, and lower flip angles can reduce the SAR by keeping the same time schedule.[65] Tailored RF pulses are designed to cancel B1 variations by maintaining the same flip angle throughout the FOV.[66] Nonselective tailored RF pulses (kT-points) were recently used to obtain T2-weighted images with uniform contrast throughout the whole brain.[67]

Relaxation Time Variation

Relaxation times change with the field strength: T1 values increase along with the field strength and then converge to a specific tissue-dependent value. T2* values decrease with field strength, leading to a loss of signal but enhancing the

sensitivity to deoxygenated blood and iron deposits. For spin-echo sequences, apparent T2 values also shortened due to diffusion effects through small local gradient variations in capillaries that depend on the tissue type. T2 values also decrease but the reduction is dependent on the type of tissue (gray/white matter).[68]

Heuristic equations of the changes of T1 and T2* for cortical gray matter are given here.[4]

A method to maximize the signal intensity would be to have a longer time to repeat (TR) and shorter time to echo (TE).

A fundamental problem inherent to FLAIR imaging is the lengthening of T1 constants of gray and white matter, while the T1 of CSF is field-independent. This has two detrimental effects. First, the desired T2 contrast is compromised, as the prolonged T1 values significantly increase T1 weighting in FLAIR images that counterbalances the T2 weighting. Second, the gain in SNR is suboptimal, as part of the gain in magnetization obtained by the increased field strength is lost by the reduced magnetization recovery at the moment of excitation.

Conclusion

Seven tesla MRI scanners produce images with exceptional SNR, high contrast, and unprecedented spatial resolution. However, several adjustments are indispensable in order to minimize image artifacts mainly caused by inhomogeneities of both B0 and B1 fields. High spatial resolution is often associated with larger imaging matrices and ultimately longer scan times, which are sometimes further extended by stricter SAR limits. Therefore, reducing image acquisition time and consequently improving patient comfort is another challenge that must be overcome in order to allow the future use of this type of scanner in the clinical setting.

References

1. Plantinga BR, Temel Y, Roebroeck A, et al. Ultra-high field magnetic resonance imaging of the basal ganglia and related structures. Front Hum Neurosci 2014;8:876.
2. Jonkman LE, Klaver R, Fleysher L, et al. Ultra-high-field MRI visualization of cortical multiple sclerosis lesions with T2 and T2*: a postmortem MRI and histopathology study. AJNR Am J Neuroradiol 2015;36:2062-7.
3. Grouiller F, Jorge J, Pittau F, et al. Presurgical brain mapping in epilepsy using simultaneous EEG and functional MRI at ultra-high field: feasibility and first results. MAGMA 2016;29:605-16.
4. Balchandani P, Naidich TP. Ultra-high-field MR neuroimaging. AJNR Am J Neuroradiol 2015;36:1204-15.
5. Lupo JM, Li Y, Hess CP, et al. Advances in ultra-high field MRI for the clinical management of patients with brain tumors. Curr Opin Neurol 2011;24:605-15.
6. Madai VI, von Samson-Himmelstjerna FC, Bauer M, et al. Ultrahigh-field MRI in human ischemic stroke–a 7 tesla study. PLoS One 2012;7:e37631.
7. Hoult DI, Richards RE. The signal-to-noise ratio of the nuclear magnetic resonance experiment. 1976. J Magn Reson 2011;213:329-43.
8. Vaughan JT, Garwood M, Collins CM, et al. 7T vs. 4T: RF power, homogeneity, and signal-to-noise comparison in head images. Magn Reson Med 2001;46:24-30.
9. Yacoub E, Shmuel A, Pfeuffer J, et al. Imaging brain function in humans at 7 Tesla. Magn Reson Med 2001;45:588-94.
10. Gruetter R, Weisdorf SA, Rajanayagan V, et al. Resolution improvements in in vivo 1H NMR spectra with increased magnetic field strength. J Magn Reson 1998;135:260-4.
11. Gati JS, Menon RS, Ugurbil K, et al. Experimental determination of the BOLD field strength dependence in vessels and tissue. Magn Reson Med 1997;38:296-302.
12. Nielsen AS, Kinkel RP, Madigan N, et al. Contribution of cortical lesion subtypes at 7T MRI to physical and cognitive performance in MS. Neurology 2013;81:641-9.
13. Harrison DM, Oh J, Roy S, et al. Thalamic lesions in multiple sclerosis by 7T MRI: clinical implications and relationship to cortical pathology. Mult Scler 2015;21:1139-50.
14. Ge Y, Zohrabian VM, Grossman RI. Seven-Tesla magnetic resonance imaging: new vision of microvascular abnormalities in multiple sclerosis. Arch Neurol 2008;65:812-6.
15. Dula AN, Pawate S, Dortch RD, et al. Magnetic resonance imaging of the cervical spinal cord in multiple sclerosis at 7T. Mult Scler 2016;22:320-8.
16. Moser E, Stahlberg F, Ladd ME, et al. 7-T MR–from research to clinical applications? NMR Biomed 2012;25:695-716.
17. Sati P, Oh J, Constable RT, et al. The central vein sign and its clinical evaluation for the diagnosis of multiple sclerosis: a consensus statement from the North American Imaging in Multiple Sclerosis Cooperative. Nat Rev Neurol 2016;12:714-22.
18. Honkanen P, Frosen JK, Abo-Ramadan U, et al. Visualization of luminal thrombosis and mural iron accumulation in giant aneurysms with ex vivo 4.7T magnetic resonance imaging. Surg Neurol Int 2014;5:74.
19. Theysohn JM, Maderwald S, Kraff O, et al. Subjective acceptance of 7 Tesla MRI for human imaging. MAGMA 2008;21:63-72.
20. de Vocht F, Stevens T, Glover P, et al. Cognitive effects of head-movements in stray fields generated by a 7 Tesla whole-body MRI magnet. Bioelectromagnetics 2007;28:247-55.
21. Chakeres DW, Kangarlu A, Boudoulas H, et al. Effect of static magnetic field exposure of up to 8 Tesla on sequential human vital sign measurements. J Magn Reson Imaging 2003;18:346-52.
22. Trampel R, Reimer E, Huber L, et al. Anatomical brain imaging at 7T using two-dimensional GRASE. Magn Reson Med 2014;72:1291-301.
23. Norris DG, Boyacioglu R, Schulz J, et al. Application of PINS radiofrequency pulses to reduce power deposition in RARE/turbo spin echo imaging of the human head. Magn Reson Med 2014;71:44-9.
24. Eggenschwiler F, O'Brien KR, Gallichan D, et al. 3D T 2-weighted imaging at 7T using dynamic kT-points on single-transmit MRI systems. MAGMA 2016;29:347-58.
25. Fiocchi S, Markakis IA, Ravazzani P, et al. SAR exposure from UHF RFID reader in adult, child, pregnant woman, and fetus anatomical models. Bioelectromagnetics 2013;34:443-52.
26. O'Brien KR, Kober T, Hagmann P, et al. Robust T1-weighted structural brain imaging and morphometry at 7T using MP2RAGE. PLoS One 2014;9:e99676.
27. De Coene B, Hajnal JV, Gatehouse P, et al. MR of the brain using fluid-attenuated inversion recovery (FLAIR) pulse sequences. AJNR Am J Neuroradiol 1992;13:1555-64.
28. Zwanenburg JJ, Hendrikse J, Visser F, et al. Fluid attenuated inversion recovery (FLAIR) MRI at 7.0 Tesla: comparison with 1.5 and 3.0 Tesla. Eur Radiol 2010;20:915-22.
29. Visser F, Zwanenburg JJ, Hoogduin JM, et al. High-resolution magnetization-prepared 3D-FLAIR imaging at 7.0 Tesla. Magn Reson Med 2010;64:194-202.
30. In MH, Posnansky O, Beall EB, et al. Distortion correction in EPI using an extended PSF method with a reversed phase gradient approach. PLoS One 2015;10:e0116320.
31. Heidemann RM, Porter DA, Anwander A, et al. Diffusion imaging in humans at 7T using readout-segmented EPI and GRAPPA. Magn Reson Med 2010;64:9-14.
32. Jeong HK, Gore JC, Anderson AW. High-resolution human diffusion tensor imaging using 2-D navigated multishot SENSE EPI at 7 T. Magn Reson Med 2013;69:793-802.
33. Schweser F, Deistung A, Lehr BW, et al. Differentiation between diamagnetic and paramagnetic cerebral lesions based on magnetic susceptibility mapping. Med Phys 2010;37:5165-78.

34. Wu Z, Mittal S, Kish K, et al. Identification of calcification with MRI using susceptibility-weighted imaging: a case study. J Magn Reson Imaging 2009;29:177-82.
35. Sanchez-Panchuelo RM, Francis S, Bowtell R, et al. Mapping human somatosensory cortex in individual subjects with 7T functional MRI. J Neurophysiol 2010;103:2544-56.
36. Schafer A, Wharton S, Gowland P, et al. Using magnetic field simulation to study susceptibility-related phase contrast in gradient echo MRI. Neuroimage 2009;48:126-37.
37. Wang Y, Liu T. Quantitative susceptibility mapping (QSM): decoding MRI data for a tissue magnetic biomarker. Magn Reson Med 2015;73:82-101.
38. Bian W, Banerjee S, Kelly DA, et al. Simultaneous imaging of radiation-induced cerebral microbleeds, arteries and veins, using a multiple gradient echo sequence at 7 Tesla. J Magn Reson Imaging 2015;42:269-79.
39. Harteveld AA, De Cocker LJ, Dieleman N, et al. High-resolution postcontrast time-of-flight MR angiography of intracranial perforators at 7.0 Tesla. PLoS One 2015;10:e0121051.
40. Zhang Z, Deng X, Weng D, et al. Segmented TOF at 7 T MRI: technique and clinical applications. Magn Reson Imaging 2015;33:1043-50.
41. Madai VI, von Samson-Himmelstjerna FC, Sandow N, et al. Ultrahigh-field MPRAGE magnetic resonance angiography at 7.0 T in patients with cerebrovascular disease. Eur J Radiol 2015;84:2613-7.
42. Tkac I, Oz G, Adriany G, et al. In vivo 1H NMR spectroscopy of the human brain at high magnetic fields: metabolite quantification at 4T vs. 7T. Magn Reson Med 2009;62:868-79.
43. Mekle R, Mlynarik V, Gambarota G, et al. MR spectroscopy of the human brain with enhanced signal intensity at ultrashort echo times on a clinical platform at 3T and 7T. Magn Reson Med 2009;61:1279-85.
44. Moenninghoff C, Kraff O, Schlamann M, et al. Assessing a dysplastic cerebellar gangliocytoma (Lhermitte-Duclos disease) with 7T MR imaging. Korean J Radiol 2010;11:244-8.
45. Ogawa S, Tank DW, Menon R, et al. Intrinsic signal changes accompanying sensory stimulation: functional brain mapping with magnetic resonance imaging. Proc Natl Acad Sci USA 1992;89:5951-5.
46. van der Zwaag W, Francis S, Head K, et al. fMRI at 1.5, 3 and 7 T: characterising BOLD signal changes. Neuroimage 2009;47:1425-34.
47. Beisteiner R, Robinson S, Wurnig M, et al. Clinical fMRI: evidence for a 7T benefit over 3T. Neuroimage 2011;57:1015-21.
48. Duong TQ, Yacoub E, Adriany G, et al. Microvascular BOLD contribution at 4 and 7 T in the human brain: gradient-echo and spin-echo fMRI with suppression of blood effects. Magn Reson Med 2003;49:1019-27.
49. Geissler A, Matt E, Fischmeister F, et al. Differential functional benefits of ultra highfield MR systems within the language network. Neuroimage 2014;103:163-70.
50. Roschmann P. Radiofrequency penetration and absorption in the human body: limitations to high-field whole-body nuclear magnetic resonance imaging. Med Phys 1987;14:922-31.
51. Hoult DI, Chen CN, Sank VJ. The field dependence of NMR imaging. II. Arguments concerning an optimal field strength. Magn Reson Med 1986;3:730-46.
52. Robitaille PM, Abduljalil AM, Kangarlu A. Ultra high resolution imaging of the human head at 8 tesla: 2K x 2K for Y2K. J Comput Assist Tomogr 2000;24:2-8.
53. Roemer PB, Edelstein WA, Hayes CE, et al. The NMR phased array. Magn Reson Med 1990;16:192-225.
54. Gagoski BA, Bilgic B, Eichner C, et al. RARE/turbo spin echo imaging with Simultaneous Multislice Wave-CAIPI. Magn Reson Med 2015;73:929-38.
55. Lee T, Cai LX, Lelyveld VS, et al. Molecular-level functional magnetic resonance imaging of dopaminergic signaling. Science 2014;344:533-5.
56. Zhang X, Liu J, Schmitter S, et al. Predicting temperature increase through local SAR estimation by B1 mapping: a phantom validation at 7T. Conf Proc IEEE Eng Med Biol Soc 2014;2014: 1107-10.
57. Schneider E, Glover G. Rapid in vivo proton shimming. Magn Reson Med 1991;18:335-47.
58. Gruetter R. Automatic, localized in vivo adjustment of all first- and second-order shim coils. Magn Reson Med 1993;29: 804-11.
59. Taylor DG, Bushell MC. The spatial mapping of translational diffusion coefficients by the NMR imaging technique. Phys Med Biol 1985;30:345-9.
60. Teeuwisse WM, Brink WM, Haines KN, et al. Simulations of high permittivity materials for 7 T neuroimaging and evaluation of a new barium titanate-based dielectric. Magn Reson Med 2012;67: 912-8.
61. Schaller B, Xin L, Gruetter R. Is the macromolecule signal tissue-specific in healthy human brain? A (1)H MRS study at 7 Tesla in the occipital lobe. Magn Reson Med 2014;72:934-40.
62. Saekho S, Yip CY, Noll DC, et al. Fast-kz three-dimensional tailored radiofrequency pulse for reduced B1 inhomogeneity. Magn Reson Med 2006;55:719-24.
63. de Greef M, Ipek O, Raaijmakers AJ, et al. Specific absorption rate intersubject variability in 7T parallel transmit MRI of the head. Magn Reson Med 2013;69:1476-85.
64. Saranathan M, Tourdias T, Kerr AB, et al. Optimization of magnetization-prepared 3-dimensional fluid attenuated inversion recovery imaging for lesion detection at 7 T. Invest Radiol 2014;49:290-8.
65. Cloos MA, Boulant N, Luong M, et al. kT -points: short three-dimensional tailored RF pulses for flip-angle homogenization over an extended volume. Magn Reson Med 2012;67:72-80.
66. Rooney WD, Johnson G, Li X, et al. Magnetic field and tissue dependencies of human brain longitudinal 1H2O relaxation in vivo. Magn Reson Med 2007;57:308-18.
67. Moore J, Jankiewicz M, Zeng H, et al. Composite RF pulses for B1+-insensitive volume excitation at 7 Tesla. J Magn Reson 2010;205:50-62.
68. Cox EF, Gowland PA. Simultaneous quantification of T2 and T'2 using a combined gradient echo-spin echo sequence at ultrahigh field. Magn Reson Med 2010;64:1440-5.